In Silico Approach for Developing New Anti-Tuberculosis Drug Candidates: 3D-QSAR, Molecular Docking and ADME Studies of Pretomanid Derivatives

A. Belafriekh[a,*], A. Laoud[b], L. El mchichi[c] and M. Bouachrine[c]

aChemistry Department, Faculty of Sciences, University of Blida 1, BP 270 Blida, 09000, Algeria.
bChemical Engineering Department, Faculty of Chemical Engineering, University of Salah Boubnider Constantine 3, Algeria
cFaculty of Science, University of Moulay Ismail, MCNSL, Meknes, Morocco
(Received 15 November 2023, Accepted 29 January 2024)

Tuberculosis (TB) is one of the top ten causes of mortality worldwide, necessitating the discovery of new molecules with potential anti-tuberculosis activity. In this study, Pretomanid derivatives as potent anti-TB agents were collected from the literature to generate a 3D-QSAR model and conduct molecular docking. The 3D-QSAR model was successfully generated with a high regression coefficient $R^2 = 0.98$ and an excellent cross-validated determination coefficient $Q^2_{cv} = 0.51$ for the training set. Furthermore, the model developed showed good predictive ability, with a high predictive value $Q^2 = 0.75$ for the test set. The generated 3D contour cubes were applied to find the structural properties necessary to inhibit Deazaflavin-dependent nitroreductase. Then, the results were used to discover novel molecules with a potential anti-tuberculosis activity using the structure-based virtual screening. Based on successful results obtained by virtual screening, twelve compounds were selected as potential inhibitors of the Ddn with highly predicted activities, binding interactions, and acceptable ADME properties.

Keywords: Pretomanid, Molecular Docking, *Mycobacterium tuberculosis*, Virtual screening, 3D-QSAR

INTRODUCTION

Tuberculosis (TB) is caused by the bacillus *Mycobacterium tuberculosis* (*Mtb*). It remains one of the world's leading causes of death due to its high mortality and morbidity rates in recent times [1-3], particularly in countries with low resources, including regions with high poverty [4]. In 2021, the World Health Organization (WHO) reported about 10 million TB cases and an estimated 1.2 million deaths globally [5]. The WHO reaffirmed its commitment to ending the TB epidemic by 2030, as per the Sustainable Development Goals (SDGs) [6]. However, the development of multidrug-resistant tuberculosis (MDR-TB), extensively drug-resistant (XDR-TB), and totally drug-resistant tuberculosis (TDR-TB) has made the situation worse recently [7]. Tuberculosis infections by drug-sensitive strains

_____
*Corresponding author. E-mail: a.belafriekh@gmail.com

traditionally treated by drugs target cell wall synthesis or inhibit bacterial growth resulting in the selection of mutant strains that may develop drug resistance [8]. Therefore, it is necessary to identify new therapeutic targets for TB treatment and new drugs that could act on them.

Pretomanid (PA-824, see in Fig. 1) is a new class of tuberculosis drug (bicyclic nitroimidazole) that was approved by the Food and Drug Administration (FDA) in 2019 for the treatment of multidrug-resistant (MDR-TB) in combination with bedaquiline and linezolid drugs, which are still in phase III clinical evaluation [9,10].

The main objective of this research is to design and predict the activity of new hit compounds as potential inhibitors of Deazaflavin-dependent nitroreductase (Ddn) against *Mycobacterium tuberculosis* using *in silico* screening approaches.

To achieve this aim, a molecular docking and a 3D quantitative structure-activity relationship model study were performed on a series of Pretomanid derivatives as TB
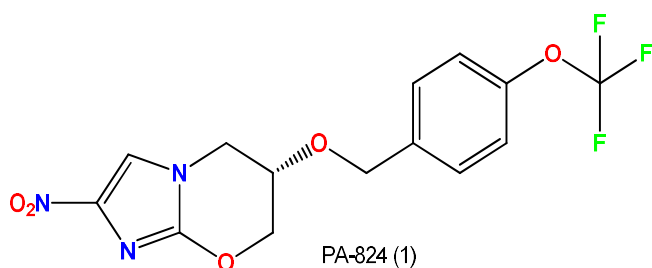
Fig. 1. Chemical structure of Pretomanid.

inhibitors to identify the structural features important for Ddn enzyme inhibition. These results were then used to discover new molecules with potential anti-tuberculosis activity using virtual screening. First, the ZINC [11] database was subjected to the Lipinski rule of five for identifying drug-like properties [12]. The resultant molecules were virtually screened using molecular docking to find the most potent inhibitors. Finally, the top hits compounds were then subjected to ADME to compare the drug-like properties with those of standard medicaments [13,14].

MATERIALS AND METHODS

Dataset

A dataset of 118 Pretomanid derivatives as TB inhibitors for this work was selected from the literature [15]. The minimum inhibitory concentration (MIC) values were converted to a logarithmic scale [$pMIC = -\log(MIC \times 10^{-6})$] (Table 1, Table 2) to reduce data skewness for the QSAR study [4]. The dataset was divided into two sets, ninety-two (92) compounds were randomly chosen as the training set for model construction, while the remaining 26 compounds were selected as the test set for external model validation [16].

Ligand Preparation

All the structures of Pretomanid derivatives are sketched using Chem draw ultra and imported to Maestro version 9.9.013 (Schrödinger) for energy minimization and generation of 3D structures using LigPrep module in Maestro [17]. The possible ionization and tautomer were generated at a pH of 7.0 ± 2.0, and energy minimizations were performed using the OPLS-2005 force field [18].

Molecular Docking

The crystal structure of Deazaflavin-dependent nitroreductase (Ddn) from *Mycobacterium tuberculosis* (PDB Id: 3R5W, resolution of 1.79 Å) was obtained from the Protein Data Bank website (www.rcsb.org) [19] and processed using protein preparation wizard module in Schrödinger [20]. All the water molecules were removed, hydrogen atoms were added, and the OPLS 2005 force field with a root mean square deviation (RMSD) value of 0.30 Å was used for optimization and minimization of the protein [21]. After the preparation of the protein, the grid box for 3R5W was generated via receptor grid generation [22]. The molecular docking studies of the ligands were carried out using Glide extra-precision (XP) mode to identify their docking score and binding mode into the active site of the Ddn enzyme [23].
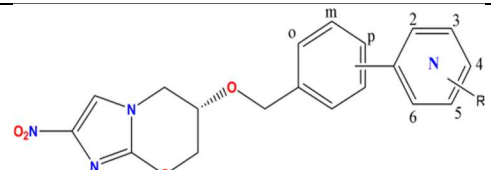
Building 3D-QSAR Model

The PHASE (version 6.1) module in Schrödinger was used to generate the atom-based 3D-QSAR model to explore the relationship between the structure of ligands and their biological activities [24,25]. All 118 compounds were split into two sets, a training set (92 compounds) and a test set (26 compounds), by using the random selection method [26] The 3D-QSAR model was generated with a maximum PLS factor of N/5 (N is the number of ligands present in the training set), hence an optimal of five of PLS factor was selected with a grid spacing of 1 Å. The best QSAR model was then validated by predicting the activity of the external dataset [27,28]. Compound 28 was selected as a reference compound to visualize the contour maps due to its stronger inhibitory activity.

Virtual Screening

The virtual screening of ZINC database was performed with the aim of discovering novel hits with potential anti-tuberculosis activity using Virtual Screening Workflow (VSW) module of Schrodinger, as shown in Fig. 2. The ZINC database was downloaded from the official site (http://zinc15.docking.org/) [11,29,30] and subjected to Lipinski's Rule of five (MW < 500, HBD < 5, HBA < 10, logP < 5) as the first filter for identifying drug-like molecules [31].

Table 1. Chemical Structures and MIC (μM) Values of Pretomanid Derivatives 1-118 [15]
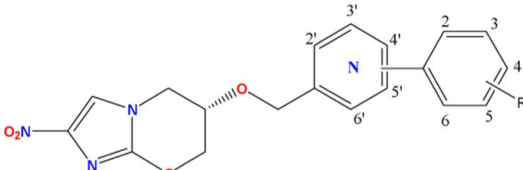

Compounds	MIC (μM)	Link	aza	R	Compounds	MIC (μM)	Link	aza	R
1	0.5	-	-	-	18	0.08	p	2	4-CN
2	0.03	p	-	CF_3	19	0.14	p	2	3-F
3	0.035	p	-	OCF_3	20	0.035	p	2	4-F
4	5.2	o	3	$4\text{-}OCH_3$	21	0.08	p	2	$4\text{-}OCF_2H$
5	2.7	o	3	$4\text{-}OCH_2Ph$	22	0.13	p	2	$4\text{-}OCH_3$
6	1.4	m	2	-	23	0.51	p	3	-
7	0.32	m	2	$4\text{-}CF_3$	24	0.03	p	3	$4\text{-}CF_3$
8	0.21	m	2	$4\text{-}OCF_2H$	25	0.20	p	3	4-CN
9	1.4	m	3	-	26	0.095	p	3	4-F
10	0.47	m	3	$4\text{-}CF_3$	27	0.55	p	3	5-F
11	0.37	m	3	4-F	28	2.6	p	3	$4\text{-}NH_2$
12	0.40	m	3	$4\text{-}OCH_3$	29	0.045	p	3	$4\text{-}OCF_2H$
13	0.07	m	3	$4\text{-}OCH_2Ph$	30	0.045	p	3	$4\text{-}OCH_3$
14	1.4	m	4	-	31	0.04	p	3	$4\text{-}OCH_2Ph$
15	0.21	p	2	-	32	0.50	p	4	-
16	0.06	p	2	$4\text{-}CF_3$	33	0.56	p	4	2-F
17	0.025	p	2	$4\text{-}CF_3, 6\text{-}Cl$	34	0.23	p	4	3-F

Compounds	MIC (μM)	Link	aza	R	Compounds	MIC (μM)	Link	aza	R
35	0.29	m	2'	$4\text{-}CF_3$	66	0.065	p	2'	$4\text{-}OCF_3$
36	0.48	m	2'	4-CN	67	0.02	p	2'	$4\text{-}OCF_2H$
37	0.30	m	2'	4-F	68	0.17	p	2'	$3\text{-}F, 4\text{-}OCH_3$
38	0.16	m	2'	$4\text{-}OCF_3$	69	0.14	p	2'	$2\text{-}Cl, 4\text{-}OCF_3$
39	0.17	m	2'	$4\text{-}OCF_2H$	70	0.04	p	2'	$3\text{-}Cl, 4\text{-}OCF_3$
40	0.30	m	2'	$3\text{-}F, 4\text{-}OCH_3$	71	0.06	p	2'	$2\text{-}F, 4\text{-}OCF_3$
41	0.71	m	2'	$3\text{-}aza, 4\text{-}OCH_3$	72	0.05	p	2'	$3\text{-}F, 4\text{-}OCF_3$
42	0.075	m	4'	$4\text{-}CF_3$	73	0.06	p	2'	$3\text{-}OCF3, 4\text{-}Cl$
43	0.38	m	4'	4-CN	74	1.4	p	2'	2-aza, 3-F
44	0.17	m	4'	4-F	75	0.83	p	2'	$2\text{-}aza, 4\text{-}CF_3$
45	0.035	m	4'	$4\text{-}OCF_3$	76	0.24	p	2'	$3\text{-}aza, 4\text{-}CF_3$

Table 1. Continued
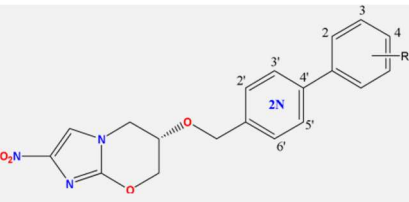
46	0.055	m	4'	4-OCF$_2$H	77	0.49	p	2'	3-aza, 4-F
47	0.34	m	4'	3-F, 4-OCH$_3$	78	2.6	p	2'	3-aza, 5-F
48	1.3	m	4'	3-aza, 4-OCH$_3$	79	0.36	p	2'	3-aza, 3-OCH$_3$
49	0.15	m	5'	4-CF$_3$	80	3.2	p	2'	4-aza, 2-F
50	0.69	m	5'	4-CN	81	1.7	p	2'	4-aza, 3-F
51	0.31	m	5'	4-F	82	0.053	p	3'	4-CF$_3$
52	0.17	m	5'	4-OCF$_3$	83	0.18	p	3'	4-CN
53	0.53	m	5'	4-OCF$_2$H	84	0.06	p	3'	4-F
54	0.91	m	5'	3-F, 4-OCH$_3$	85	0.05	p	3'	4-OCF$_3$
55	2.8	m	5'	3-aza, 4-OCH$_3$	86	0.02	p	3'	4-OCF$_2$H
56	0.88	m	6'	4-CF$_3$	87	0.09	p	3'	3-F, 4-OCH$_3$
57	2.1	m	6'	4-CN	88	0.03	p	3'	2-Cl, 4-OCF$_3$
58	0.46	m	6'	4-F	89	0.017	p	3'	3-Cl, 4-OCF$_3$
59	0.76	m	6'	4-OCF$_3$	90	0.047	p	3'	2-F, 4-OCF$_3$
60	0.67	m	6'	4-OCF$_2$H	91	0.025	p	3'	3-F, 4-OCF$_3$
61	2.3	m	6'	3-F, 4-OCH$_3$	92	0.18	p	3'	3-OCF$_3$, 4-Cl
62	3.8	m	6'	3-aza, 4-OCH$_3$	93	0.19	p	3'	3-aza, 4-CF$_3$
63	0.04	p	2'	4-CF$_3$	94	0.37	p	3'	3-aza, 4-F
64	0.18	p	2'	4-CN	95	0.24	p	3'	3-aza, 4-OCH$_3$
65	0.13	p	2'	4-F					

96	0.06		2',3'	4-CF$_3$	108	0.33		2', 5'	3-aza, 4-CF$_3$
97	0.36		2', 3'	4-CN	109	0.06		2', 6'	4-CF$_3$
98	0.19		2', 3'	4-F	110	0.13		2', 6'	4-F
99	0.075		2', 3'	4-OCF$_3$	111	0.11		2', 6'	4-OCF$_3$
100	0.17		2', 3'	4-OCF$_2$H	112	0.12		2', 6'	4-OCF$_2$H
101	0.25		2', 3'	3-F, 4-OCH$_3$	113	0.28		2', 6'	3-aza, 4-CF$_3$
102	0.55		2', 3'	3-aza, 4-CF$_3$	114	0.025		3', 5'	4-CF$_3$
103	0.72		2', 3'	3-aza, 4-OCH$_3$	115	0.11		3', 5'	4-F
104	0.08		2', 5'	4-CF$_3$	116	0.027		3', 5'	4-OCF$_3$
105	0.085		2', 5'	4-F	117	0.13		3', 5'	4-OCF$_2$H
106	0.023		2', 5'	4-OCF$_3$	118	0.16		3', 5'	3-aza, 4-CF$_3$
107	0.20		2', 5'	4-OCF$_2$H					

O: Ortho   *m: Meta*   *P: Para*

Table 2. PLS Statistics Parameters

PLS	SD	R^2	R^2_{CV}	$R^2_{Scramble}$	Stability	F	P	RMSE	Q^2	Pearson-r
1	0.45	0.47	0.29	0.40	0.95	80.8	3.64e-14	0.38	0.37	0.64
2	0.27	0.81	0.44	0.65	0.72	189.8	7.96e-33	0.24	0.74	0.86
3	0.21	0.89	0.50	0.78	0.69	241.7	2.33e-42	0.25	0.73	0.85
4	0.16	0.93	0.51	0.86	0.65	309.3	1.53e-50	0.26	0.71	0.85
5	0.12	0.98	0.51	0.91	0.61	463.9	1.3e-60	0.24	0.75	0.87

PLS: optimal number of components; SD: standard deviation of the regression; R^2: regression coefficient; F: variance ratio; P: significance level of variance ratio; Q^2: cross-validated correlation coefficient for the test set; RMSE: root-mean-square error in the test set predictions; Pearson-r, correlation between the predicted and observed activity for the test set.
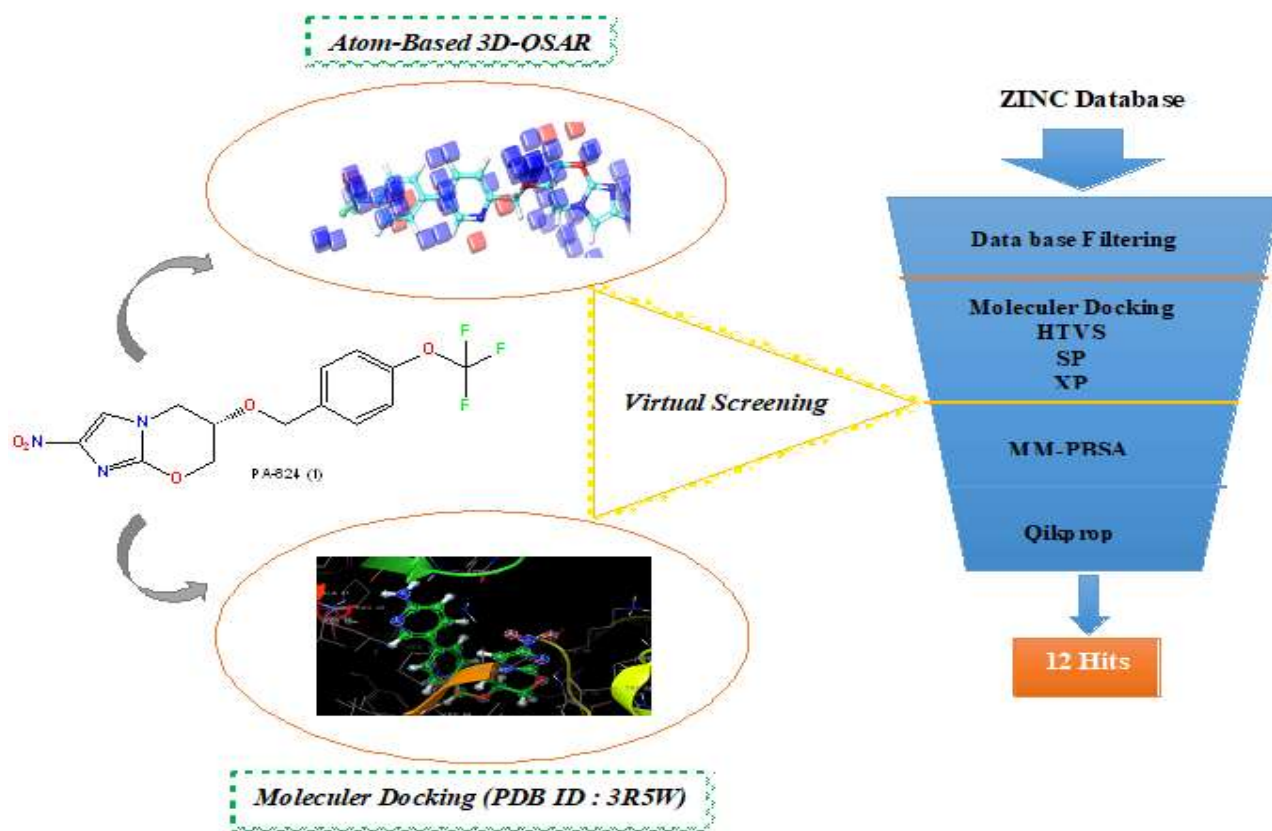

Fig. 2. Workflow for Virtual screening.

The resulting molecules from the first stage of filtration were screened by using a second filter, *i.e.* molecular docking (HTVS, SP, and XP) to find the most potent inhibitors [32]. The retrieved molecules were docked into the active site of the Ddn enzyme using the high-throughput virtual Screening (HTVS), and the best-scoring molecules 5% were selected and passed to the standard precision (SP) method. Again, 5%of the top-scoring molecules from Glide SP were selected and subjected to the extra precision (XP) method. Finally, 70 hits molecules selected with a glide score > -13.34 were then submitted to PHASE to predict the activity by using the developed 3D-QSAR model.

ADME Prediction of Hits

The resulting molecules from the molecular docking were predicted for the Absorption, Distribution, Metabolism, and Excretion (ADME) properties using the QikProp module of Schrodinger [33,34]. The analysis provides significant physicochemical properties such as MW, HBD, HBA, LogP, QPlogPw, QPlogS, QPPCaco, PHOA, QPlogPw, %HOA, QPlogKha, #rotor, QPPMDCK [35,36].

RESULTS AND DISCUSSION

Docking Analysis of Pretomanid Derivatives

The crystal structure of Ddn from *Mycobacterium tuberculosis* was retrieved and subjected to a molecular docking approach using the Glide (version 6.2) module in Schrodinger to explore the interactions between the target protein and the ligand [37]. The docking studies in the active site of Ddn revealed that Pretomanid derivatives interact with many interactions, such as pi-pi stacking, hydrogen bonds, salt bridge, and hydrophobic. For all ligands, as observed in Fig. 3, nitroimidazole formed a salt bridge interaction with LYS79 and LYS103. In addition, its pyrimidine ring observed interaction with ASN62 by hydrogen bond and a hydrophobic interaction Pi–Pi stacking with TRP88 and TYR65. The NO_2 groups showed hydrogen bond interactions with ASN62 and SER78. These interactions are essential for the inhibitions of Deazaflavin-dependent nitroreductase (Ddn). The interaction of compounds 28, 55, 14, and 1 in the active site of Ddn is shown in Fig. 3.
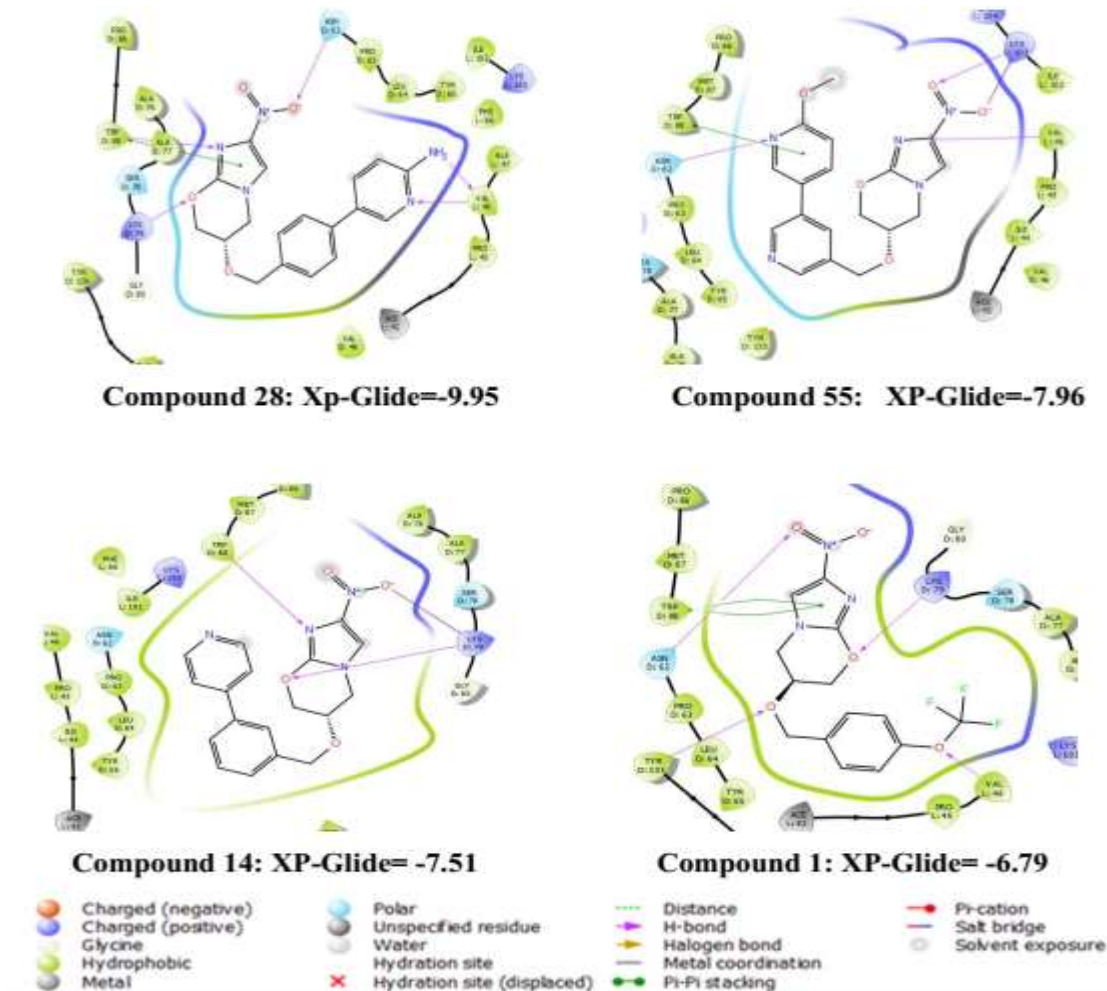

Compound 28: Xp-Glide=-9.95

Compound 55: XP-Glide=-7.96

Compound 14: XP-Glide= -7.51

Compound 1: XP-Glide= -6.79

Charged (negative)   Polar   Distance   Pi-cation
Charged (positive)   Unspecified residue   H-bond   Salt bridge
Glycine   Water   Halogen bond   Solvent exposure
Hydrophobic   Hydration site   Metal coordination
Metal   Hydration site (displaced)   Pi-Pi stacking

Fig. 3. 2D-Interaction of compounds 28, 55, 14, and 1 in the active site of Ddn (PDB: 3R5W).

3D-QSAR Model Analysis

The atom-based 3D-quantitative structure-activity relationship (QSAR) model was developed successfully, with five PLS factors having an excellent regression coefficient $R^2 = 0.98$ ($R^2 > 0.6$), a good cross-validated determination coefficient $Q^2cv = 0.51$ ($Q^2_{cv} > 0.5$) for the internal validation of training set. The model was also validated by the high predictive value for the external validation of test set $Q^2 = 0.75$ ($Q^2 > 0.6$), suggesting that the model is statistically significant and has a mighty predictive power. In addition, a large variance ratio (F) value of 463.9 indicates a more statistically significant regression, Pearson-r of 0.87, and a smaller P value (1.3e-60) with stability of the generated model 0.61 on a scale of 1 indicating a greater degree of confidence on the model. A smaller standard deviation (SD)

value of 0.12 and root mean square error (RMSE) value of 0.24 indicate that the data used to generate the model are better for QSAR analysis. A summary of the PLS statistics parameters of the model is presented in Table 2. Actual and predicted activities (pMIC), and residual values of the dataset are presented in Table 4. The graphs of actual versus predicted activities (pMIC) of training and test set molecules are presented in Fig. 4.

The contributions of a hydrogen bond donor, hydrophobic group, negative ionic, positive ionic, and electron-withdrawing group were found to be 0.4%, 42.3%, 10.4%, 10.4%, and 36.5%, respectively, which indicates that the hydrophobic and electron-withdrawing groups have the highest contribution in this model (Table 3).

Table 3. Field Contribution of the 3D-QSAR Model

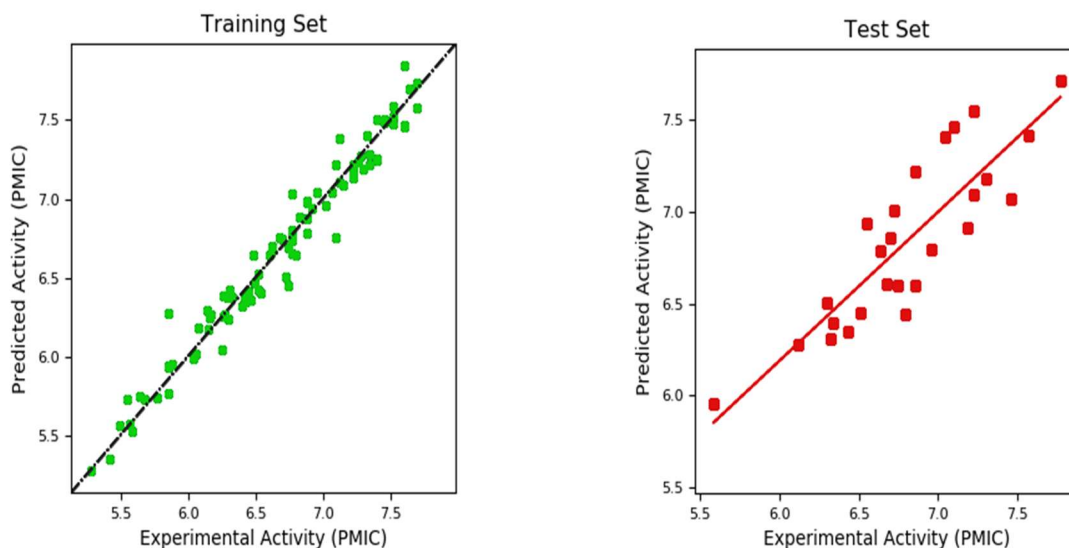| PLS	Field Contribution (%)				
	H-bond donor	Hydrophobic	Negative ionic	Positive ionic	Electron-withdrawing
1	0.3	51.0	07.7	07.9	33.1
2	0.3	46.1	09.0	09.5	35.0
3	0.3	44.3	09.6	09.9	35.8
4	0.3	42.5	10.0	10.3	36.6
5	0.4	42.3	10.5	10.4	36.5

Fig. 4. Graphs of actual *vs*. predicted activities (pMIC) of training and test set compounds.

3D-QSAR Contour Maps Analysis

To analyze 3D-QSAR results, the PHASE module of Schrödinger was used to generate the atom-based contour maps, shown in Fig. 5, with the most active compound (compound 28) as a reference. The generated 3D contour maps showed the pharmacophoric features important of compounds for inhibiting Deazaflavin-dependent nitroreductase (Ddn), including hydrogen bond donor, hydrophobic, negative/positive ionic, and electron-withdrawing features. Blue cubes indicate favorable regions and red cubes indicate unfavorable regions for Ddn inhibitor activity [38]. In the hydrogen bond donor effect, red cubes are observed only near the NH_2 group of ligands. In the hydrophobic effect, the blue cubes are presented around the $-NO_2$ group of imidazole rings. Moreover, the blue cubes are observed near the NH_2 ring group, indicating these positions favored the Ddn inhibitory activity. The negative and positive ionic showed blue cubes near the NO_2 group of the compounds. In the electron-withdrawing effect, the blue cubes are observed in the NO_2 group of imidazole rings. Moreover, blue cubes are observed in the NH_2 group of

compounds.

Virtual Screening analysis

The molecular docking analysis revealed that top hits molecules interact with active site residues of Deazaflavin-dependent nitroreductase (Ddn) analogously to Pretomanid analogs. The docking studies of the top hits molecules showed that the hydrogen bond acceptor interactions were observed with TRP88, SER78, LYS79, and ASN62 amino acid residues, and hydrogen bond donor interaction was also observed with ALA76 residue. While the pi-pi interactions occurred with TRP88 and TYR65 residues. The binding energy of the virtual screening hits, as shown in Table 5 (range: -9.95 to -13.43 kcal mol^{-1}), was better than the binding energy of the reference compound (compound 28; XP-Glide = -9.95 kcal mol^{-1}), which indicates that the virtual screening hits had strong binding interactions for the inhibition of Ddn. The interactions of the top hits molecules into site active Ddn are presented in Fig. 6, and docking values, binding interactions, and predicted activity (pMICpred) are depicted in Table 5.
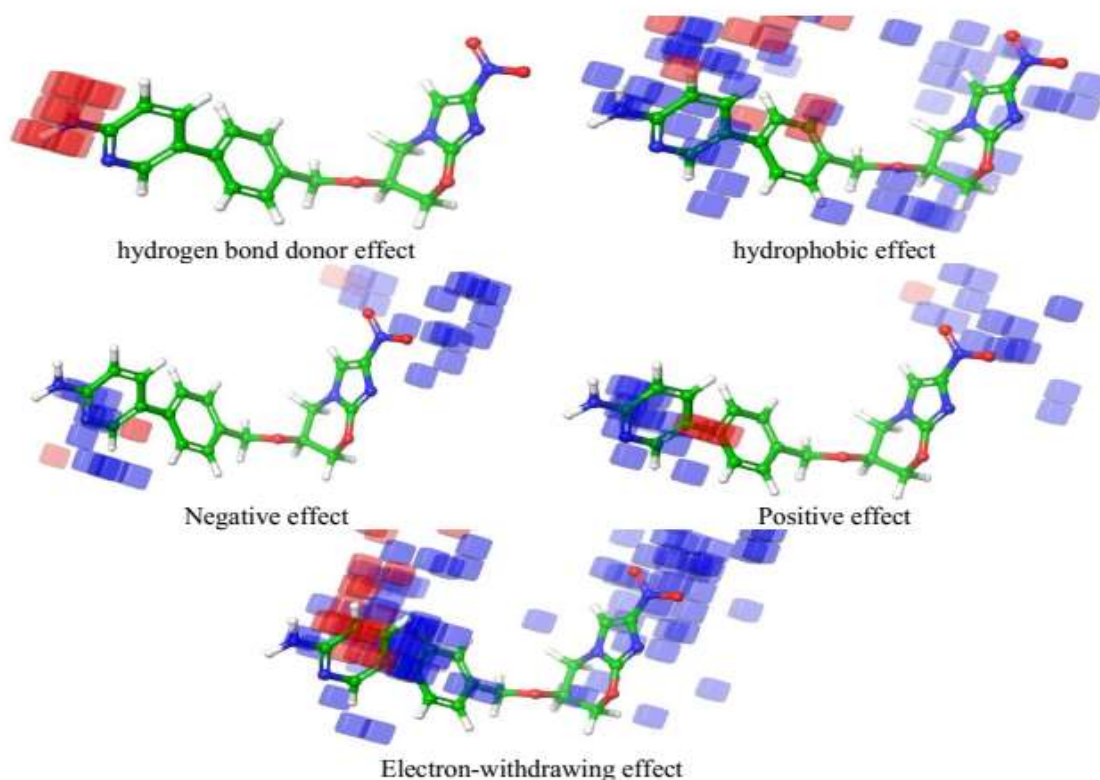

Fig. 5. Representation of the contour maps with the most active compounds (28) using the 3D-QSAR model.

Table 4. Actual pMIC $_{(Exp)}$, Predicted pMIC $_{(Pred)}$, and Residual Values of Dataset

| Compounds	pMIC$_{(Exp)}$	pMIC$_{(Pred)}$	Residual	Compounds	pMIC$_{(Exp)}$	pMIC$_{(Pred)}$	Residual
1	6.30	6.23	-0.07	60	6.17	6.27	0.09
2	7.52	7.59	0.06	61	5.64	5.75	0.11
3*	7.46	7.02	-0.39	62	5.42	5.35	-0.07
4	5.28	5.27	-0.01	63	7.40	7.51	0.11
5	5.57	5.57	-0.05	64	6.75	6.69	-0.05
6	5.85	5.94	0.09	65	6.89	6.78	-0.11
7	6.50	6.47	-0.02	66*	7.19	6.92	-0.27
8	6.68	6.75	0.08	67	7.70	7.74	0.04
9	5.85	5.93	0.08	68	6.77	6.74	-0.03
10	6.33	6.37	0.04	69*	6.85	7.22	0.37
11	6.43	6.35	-0.08	70	7.40	7.25	-0.15
12	6.40	6.32	-0.08	71	7.22	7.16	-0.06
13	7.15	7.09	-0.06	72	7.30	7.19	-0.11
14	5.85	5.76	-0.09	73	7.22	7.22	-0.00
15*	6.68	6.61	-0.07	74	5.85	6.27	0.42
16*	7.22	7.55	0.33	75	6.08	6.18	0.10
17	7.60	7.46	-0.15	76	6.62	6.67	0.05
18	7.10	7.22	0.12	77	6.31	6.43	0.12
19*	6.85	6.60	-0.26	78*	5.59	5.95	0.37
20	7.46	7.49	0.03	79	6.44	6.40	-0.04
21	7.10	6.75	-0.34	80	5.50	5.56	0.06
22	6.88	6.90	0.10	81	5.77	5.74	-0.03
23	6.29	6.38	0.09	82	7.28	7.27	-0.01
24	7.52	7.47	-0.05	83*	6.75	6.60	-0.14
25	6.70	6.74	0.04	84	7.22	7.20	-0.02
26	7.02	6.95	-0.07	85*	7.30	7.18	-0.12
27	6.26	6.39	0.13	86	7.70	7.58	-0.12
28	5.58	5.52	-0.06	87*	7.05	7.41	0.36
29	7.35	7.28	-0.06	88	7.52	7.52	-0.00
30	7.35	7.22	-0.13	89*	7.77	7.71	-0.06
31	7.40	7.25	-0.14	90	7.33	7.41	0.08
32*	6.30	6.50	0.20	91	7.60	7.85	0.25
33	6.25	6.04	-0.21	92	6.75	6.45	-0.29
34*	6.64	6.79	0.15	93*	6.72	7.01	0.28
35	6.54	6.40	-0.14	94*	6.43	6.35	-0.08
36*	6.32	6.31	-0.01	95	6.62	6.70	0.08
37	6.52	6.52	0.00	96	7.22	7.13	-0.09
38*	6.79	6.44	-0.35	97	6.44	6.41	-0.03
39	6.77	7.03	0.26	98	6.72	6.50	-0.22
40	6.52	6.42	-0.10	99	7.13	7.38	0.25
41	6.15	6.17	0.02	100	6.77	6.76	-0.01
42	7.13	7.11	-0.02	101	6.60	6.64	0.04
43	6.42	6.38	-0.01	102	6.26	6.26	-0.00
44	6.77	6.65	-0.12	103	6.14	6.30	0.15
45	7.46	7.50	0.05	104*	7.10	7.47	0.37
46	7.26	7.24	-0.02	105	7.07	7.04	-0.03
47	6.47	6.36	-0.11	106	7.64	7.70	0.06
48	5.89	5.83	-0.06	107*	6.70	6.86	0.16
49	6.82	6.89	0.06	108	6.48	6.65	0.17
50	6.16	6.25	0.08	109*	7.22	7.09	-0.13
51*	6.51	6.45	-0.06	110	6.89	6.98	0.09
52	6.77	6.80	0.03	111*	6.96	6.79	-0.17
53	6.28	6.27	-0.01	112	6.92	6.94	0.02
54	6.04	5.73	0.18	113*	6.55	6.93	0.38
55	5.55	5.59	0.04	114	7.60	7.47	-0.14
56	6.06	6.02	-0.04	115	6.69	7.04	0.08
57	5.69	5.73	0.05	116*	7.57	7.41	-0.16
58*	6.34	6.40	0.06	117	6.88	6.87	-0.01
59*	6.12	6.28	0.16	118	6.80	6.65	-0.15

*Test set
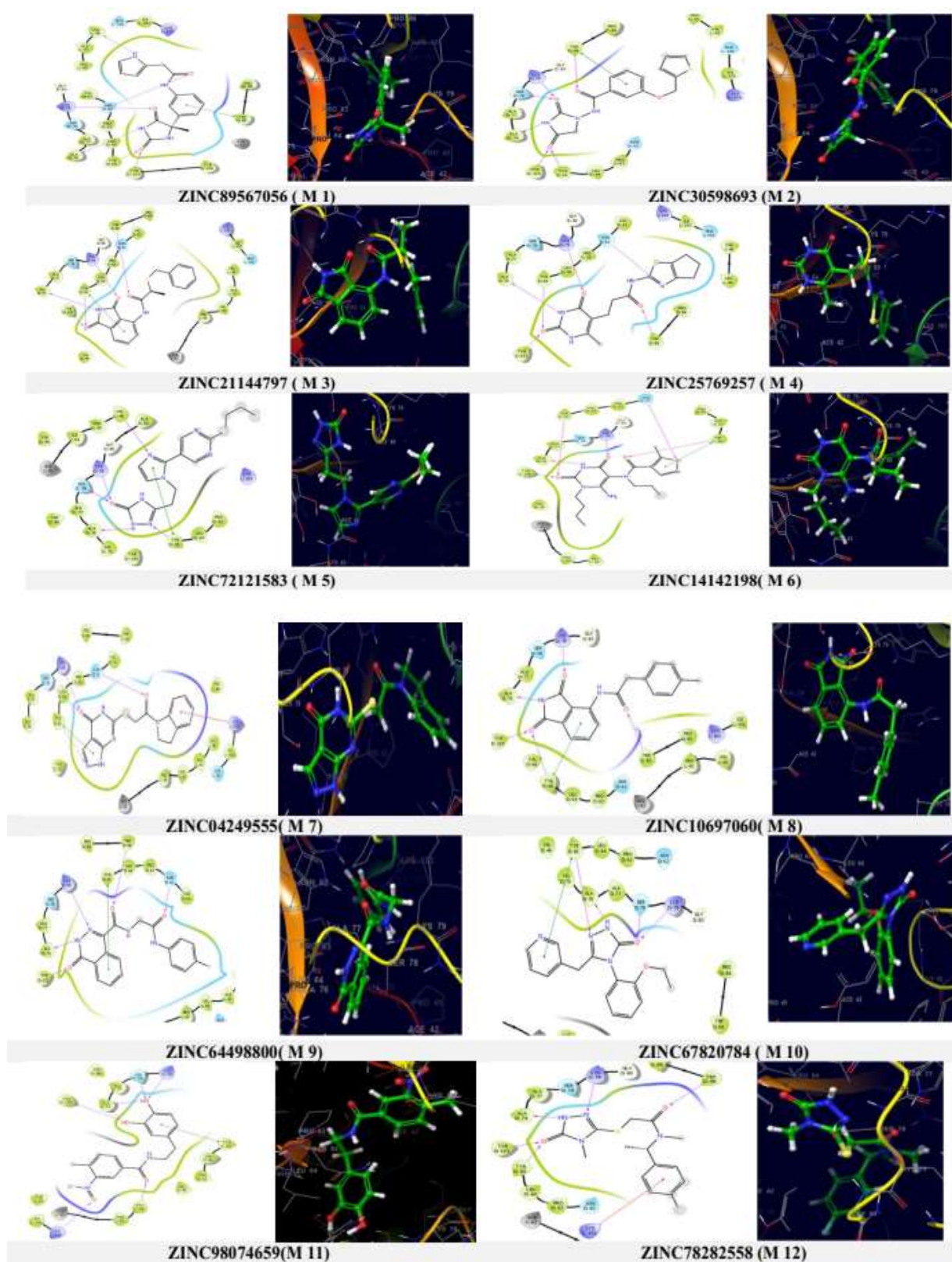
Fig. 6. 2D-interactions and 3D-interactions of the top hits in the site active of Dnd (PDB: 3R5W).

Table 5. Docking Values, Binding Interactions, and Predicted Activity PMIC$_{pred}$ of the Top Hits Molecules

Hits	XP-Score	Glide E-model	MMGBSA	Interacting residues (length in A°)	PMIC$_{pred}$
M 1	-13.34	-71.28	-59.09	HBA = ASN62 (2.36), LYS79 (1.77), TYR65 (1.77), TYR133 (2.37); HBD = ALA76 (1.89) VAL46 (1.98); Pi-Pi = TRP88 (4.91)	5.62
M 2	-12.84	-81.98	-51.76	HBA = SER78 (1.94), LYS79 (1.80), TYR65 (1.76), TYR133 (2.27), TRP88 (2.00); HBD = ALA76 (1.99); Pi-Pi = TRP88 (5.00)	5.90
M 3	-11.65	-77.52	-64.93	HBA = TRP88 (1.81), LYS79 (1.85), TYR65(2.18), TYR133 (1.87); HBD = ALA76 (1.78); Pi-Pi = TYR65 (5.45)	5.98
M 4	-10.76	-72.80	-45.50	HBA = ASN62 (2.54), LYS79 (1.80), TYR133 (1.88), TYR65 (2.00), TRP88 (2.60); HBD = ALA76 (2.09)	5.99
M 5	-10.75	-69.39	-50.90	HBA = SER78 (2.41), LYS79 (2.13), TYR65 (2.19), VAL46 (2.52); HBD = ALA76 (2.70); Pi-Pi = TYR65 (5.28)	6.50
M 6	-10.68	-80.97	-54.24	HBA = ASN62 (1.82), LYS79 (1.79), TYR133 (2.03), TYR65 (2.02), TRP88 (2.12); HBD = ALA76 (2.14); Pi-Pi = TRP88 (5.17)	6.01
M 7	-10.62	-62.33	-47.11	HBA = ASN62 (1.80), LYS79 (1.78), SER78 (2.44), TYR65 (2.09); Pi-Pi = TYR65 (5.08); Pi-cation = LYS103 (6.32)	6.13
M 8	-10.47	-70.99	-52.50	HBA = TRP88 (2.00), LYS79 (1.89), TYR65 (2.18), TYR133 (1.77); HBD = ALA76 (1.73); pi-pi = TYR65 (5.28)	6.26
M 9	-10.45	-81.40	-53.02	HBA = ASN62 (1.97), TRP88 (1.78), LYS79 (2.66), TYR133 (1.70); HBD = ALA76 (1.80); pi-pi = TYR65 (5.02)	5.90
M 10	-10.40	-61.83	-60.29	HBA = SER78 (2.54), LYS79 (2.07), TYR65 (2.18); HBD = ALA76 (2.06); pi-pi = TYR65 (5.20)	6.30
M 11	-10.31	-78.29	-58.25	HBA = SER78 (2.23), LYS79 (2.37), VAL46 (2.65), LYS133 (1.83), LYS103 (2.25); HBD = ALA76 (1.38, 1.68); Pi-Pi = TYR65(5.49).	6.43
M 12	-9.95	-66.76	-56.46	HBA = TRP88 (2.01), LYS79 (2.59), TYR65 (2.05), TYR133 (1.97); HBD = ALA76 (1.67); Pi-cation = LYS103 (6.42)	6.19

ADME Prediction of Hits

ADME properties values of the top hits compounds were calculated using Qikprop and found to be within the acceptable range, which indicates the best drug-like compounds and pharmacokinetic characteristics (Table 6).

CONCLUSION

In the current research, the 3D-quantitative structure-activity relationship (QSAR) model combined with molecular docking was conducted on a series of PA-824

Table 6. ADME Properties of the Top Hits

Hits	MW[a]	dHB[b]	aHB[C]	logP[d]	QPlogPw[e]	QPlogS[f]	QPPCaco[g]	PHOA[h]	HOA[i]	QPlogKha[j]	#rotor[k]	QPPMDCK[l]
M 1	312.33	3	5	1.84	12.68	-3.95	169.58	77.65	3	0.03	3	72.68
M 2	331.35	1.25	6	2.35	10.77	-3.96	274.37	84.36	3	-0.10	5	221.93
M 3	340.40	1	5	3.10	9.68	-4.69	295.42	89.32	3	0.25	5	174.05
M 4	320.36	3	7.5	0.87	13.5	-3.67	133.84	70.06	3	-0.33	4	104.83
M 5	331.39	2	6.5	2.15	11.93	-4.90	127.76	77.26	3	0.02	6	85.63
M 6	349.39	3	8.5	1.46	14.36	-4.13	157.48	74.83	3	-0.30	8	67.09
M 7	327.36	2	7.5	1.54	13.79	-3.85	154.70	75.18	3	-0.19	3	103.92
M 8	294.31	1	4.5	2.42	9.02	-3.96	358.20	86.81	3	0.13	3	163.09
M 9	340.31	1.25	5.25	2.60	10.79	-4.87	135.92	80.37	3	0.18	4	103.30
M 10	296.33	1	5.25	2.70	9.73	-4.12	613.07	92.64	3	0.10	4	291.52
M 11	316.31	3	5	1.49	12.04	-3.87	58.37	67.30	3	-0.02	7	22.96
M 12	324.37	1	6	1.82	11.16	-3.34	255.85	80.68	3	-0.37	5	457.98
PA-824	359.26	0	5.2	3.05	7.36	-4.20	607.85	94.63	3	-0.10	5	1352.49
28	367.36	2	6.7	2.27	12.95	-4.61	91.13	75.29	3	0.10	6	37.14
Acceptable range	< 500	0-6	2-20	-2 to 6.5	4-45	-6.5 to 0.5	<25 poor, >500 great	80% high, 25% low	1 low, 3 high	-1.5 to 1.5	0-15	<25 poor, >500 great

[a]molecular weight; [b]hydrogen bond donors; [C]hydrogen bond acceptors; [d]predicted octanol/water partition coefficient; [e]predicted water/gas partition coefficient; [f]predicted aqueous solubility, logarithm in mol dm^{-3} ; [g]predicted apparent Caco-2 cell permeability in nm s^{-1}; [h]percent human oral absorption; [i]human oral absorption; [j]Prediction of binding to human serum albumin; [k]Number of non-trivial, non-hindered rotatable bonds; [l]Predicted apparent MDCK cell permeability in nm s^{-1}.

derivatives as Ddn inhibitors. The docking analysis showed better interactions of the dataset with amino acid residues such as TRP88, ASN62, LYS79, TYR65, and TYR133. The 3D-QSAR model showed an excellent correlation coefficient ($R^2 = 0.98$), and cross-validation coefficient ($Q^2_{cv} = 0.51$) with small RMSE (0.24) and SD (0.12) at 5 factors PLS level. The good predictive power ($Q^2 = 0.75$) of this model was validated by a test set. Finally, twelve new hit compounds as potential inhibitors of the Ddn enzyme were identified from the ZINC database by *in silico* screening approaches.

ACKNOWLEDGEMENTS

REFERENCES

[1] Laoud, A.; Ali-Rachedi, F.; Ferkous, F., Discovery of New Inhibitors of Enoyl-ACP Reductase *via* Structure-Based Virtual Screening. *Phys. Chem. Res.* **2023**, *11* (3), 459-469. https://doi.org/10.22036/pcr.2022.342259.2106.

[2] Sawy, M. A. El; Elshatanofy, M. M.; Kilany, Y. El; Kandeel, K.; Elwakil, B. H.; Hagar, M.; Aouad, M. R.; Albelwi, F. F.; Rezki, N.; Jaremko, M.; Sayed, E.; Ashry, H. El, Mycobacterium Tuberculosis Enoyl Acyl Carrier Protein Reductase (InhA): Design , Synthesis , and Molecular Docking. *Int. J. Mol. Sci.* **2022**. *23*, 4706. https://doi.org/https://doi.org/10.3390/ijms23094706.

[3] Wang, X.; Ahn, Y. -M.; Lentscher, A. G.; Lister, J. S.; Brothers, R. C.; Kneen, M. M.; Gerratana, B.; Boshoff, H. I.; Dowd, C. S., Design, Synthesis, and Evaluation of Substituted Nicotinamide Adenine Dinucleotide (NAD+) Synthetase Inhibitors as Potential Antitubercular Agents. *Bioorg. Med. Chem. Lett.* **2017**, *27* (18), 4426-4430. https://doi.org/https://doi.org/10.1016/j.bmcl.2017.08.012.

[4] Abdullahi, M.; Uzairu, A.; Shallangwa, G. A.; Mamza,

P. A.; Ibrahim, M. T., 2D-QSAR, 3D-QSAR, Molecular Docking and ADMET Prediction Studies of Some Novel 2-((1H-Indol-3-Yl)Thio)-N-Phenyl-Acetamide Derivatives as Anti-Influenza A Virus. *Egypt. J. Basic Appl. Sci.* **2022**, *9* (1), 510-532. https://doi.org/10.1080/2314808X.2022.2108592.

[5] World Health Organization. Global tuberculosis report, 2021. *Https://Www.Who.Int/Teams/Global-Tuberculosis-Programme/Tb-Reports*, **2021**. https://www.who.int/teams/global-tuberculosis-programme/tb-reports.

[6] Zhang, D.; Lin, Y.; Chen, X.; Zhao, W.; Chen, D.; Gao, M.; Wang, Q.; Wang, B.; Huang, H.; Lu, Y.; Lu, Y., Docking- and Pharmacophore-Based Virtual Screening for the Identification of Novel Mycobacterium Tuberculosis Protein Tyrosine Phosphatase B (MptpB) Inhibitor with a Thiobarbiturate Scaffold. *Bioorg. Chem.* **2019**, *85* (September 2018), 229-239. https://doi.org/10.1016/j.bioorg.2018.12.038.

[7] Sharma, D.; Bisht, D. M., Tuberculosis Hypothetical Proteins and Proteins of Unknown Function: Hope for Exploring Novel Resistance Mechanisms as Well as Future Target of Drug Resistance. *Front. Microbiol.* **2017**, *8* (MAR), 1-5. https://doi.org/10.3389/fmicb.2017.00465.

[8] Saxena, S.; Abdullah, M.; Sriram, D.; Guruprasad, L., Discovery of Novel Inhibitors of Mycobacterium Tuberculosis Murg: Homology Modelling, Structure Based Pharmacophore, Molecular Docking, and Molecular Dynamics Simulations. *J. Biomol. Struct. Dyn.* **2018**, *36* (12), 3184-3198. https://doi.org/10.1080/07391102.2017.1384398.

[9] Occhineri, S.; Matucci, T.; Rindi, L.; Tiseo, G.; Falcone, M.; Riccardi, N.; Besozzi, G., Pretomanid for Tuberculosis Treatment: An Update for Clinical Purposes. *Curr. Res. Pharmacol. Drug Discov.* **2022**, *3*, 100128. https://doi.org/10.1016/j.crphar.2022.100128.

[10] Stancil, S. L.; Mirzayev, F.; Abdel-Rahman, S. M., Profiling Pretomanid as a Therapeutic Option for TB Infection: Evidence to Date. *Drug Des. Devel. Ther.* **2021**, *15*, 2815-2830. https://doi.org/10.2147/DDDT.S281639.

[11] Irwin, J. J.; Shoichet, B. K., ZINC-A Free Database of Commercially Available Compounds for Virtual Screening. *J. Chem. Inf. Model.* **2005**, *45* (1), 177-182. https://doi.org/10.1021/ci049714+.

[12] Lipinski, C. A., Drug-like Properties and the Causes of Poor Solubility and Poor Permeability. *J. Pharmacol. Toxicol. Methods* **2000**, *44* (1), 235-249. https://doi.org/10.1016/s1056-8719(00)00107-6.

[13] Bhattacharya, S.; Asati, V.; Ali, A.; Ali, A.; Gupta, G. D., *In-Silico* Studies for the Development of Novel RET Inhibitors for Cancer Treatment. *J. Mol. Struct.* **2022**, *1251*, 132040. https://doi.org/https://doi.org/10.1016/j.molstruc.2021.132040.

[14] Khamouli, S.; Belaidi, S.; Ouassaf, M.; Lanez, T.; Belaaouad, S.; Chtita, S., Multi-Combined 3D-QSAR, Docking Molecular and ADMET Prediction of 5-Azaindazole Derivatives as LRRK2 Tyrosine Kinase Inhibitors. *J. Biomol. Struct. Dyn.* **2022**, *40* (3), 1285-1298. https://doi.org/10.1080/07391102.2020.1824815.

[15] Kmentova, I.; Sutherland, H. S.; Palmer, B. D.; Blaser, A.; Franzblau, S. G.; Wan, B.; Wang, Y.; Ma, Z.; Denny, W. A.; Thompson, A. M., Synthesis and Structure-Activity Relationships of Aza- and Diazabiphenyl Analogues of the Antitubercular Drug (6S)-2-Nitro-6-{[4-(Trifluoromethoxy)Benzyl]Oxy}-6,7-Dihydro-5H-Imidazo[2,1-b][1,3]Oxazine (PA-824). *J. Med. Chem.* **2010**, *53* (23), 8421-8439. https://doi.org/10.1021/jm101288t.

[16] Luo, X.; Zhao, Y.; Tang, P.; Du, X.; Li, F.; Wang, Q.; Li, R.; He, J., Discovery of New Small-Molecule Cyclin-Dependent Kinase 6 Inhibitors through Computational Approaches. *Mol. Divers.* **2021**, *25* (1), 367-382. https://doi.org/10.1007/s11030-020-10120-3.

[17] Aloyuni, S. A., *In Silico* Prediction of Deleterious Single Nucleotide Polymorphism in Human AKR1C3 Gene and Identification of Potent Inhibitors Using Molecular Docking Approach. *J. King Saud Univ. -Sci.* **2021**, *33* (6), 101514. https://doi.org/https://doi.org/10.1016/j.jksus.2021.101514.

[18] Azam, M. A.; Thathan, J.; Jupudi, S., Pharmacophore Modeling, Atom Based 3D-QSAR, Molecular Docking and Molecular Dynamics Studies on Escherichia Coli ParE Inhibitors. *Comput. Biol. Chem.* **2020**, *84*, 107197. https://doi.org/10.1016/j.compbiolchem.2019.107197.

[19] Cellitti, S. E.; Shaffer, J.; Jones, D. H.; Mukherjee, T.; Gurumurthy, M.; Bursulaya, B.; Boshoff, H. I.; Choi, I.; Nayyar, A.; Lee, Y. S.; Cherian, J.; Niyomrattanakit, P.; Dick, T.; Manjunatha, U. H.; Barry, C. E., 3rd; Spraggon, G.; Geierstanger, B. H. Structure of Ddn, the Deazaflavin-Dependent Nitroreductase from Mycobacterium Tuberculosis Involved in Bioreductive Activation of PA-824. *Structure* **2012**, *20* (1), 101-112. https://doi.org/10.1016/j.str.2011.11.001.

[20] Chinnasamy, S.; Selvaraj, G.; Selvaraj, C.; Kaushik, A. C.; Kaliamurthi, S.; Khan, A.; Singh, S. K.; Wei, D. -Q., Combining *in Silico* and *in Vitro* Approaches to Identification of Potent Inhibitor against Phospholipase A2 (PLA2). *Int. J. Biol. Macromol.* **2020**, *144*, 53-66. https://doi.org/10.1016/j.ijbiomac.2019.12.091.

[21] Bharadwaj, K. K.; Ahmad, I.; Pati, S.; Ghosh, A.; Sarkar, T.; Rabha, B.; Patel, H.; Baishya, D.; Edinur, H. A.; Abdul Kari, Z.; Ahmad Mohd Zain, M. R.; Wan Rosli, W. I., Potent Bioactive Compounds From Seaweed Waste to Combat Cancer Through Bioinformatics Investigation. *Front. Nutr.* **2022**, *9*, 889276. https://doi.org/10.3389/fnut.2022.889276.

[22] Nair, S. B.; Teli, M. K.; Pradeep, H.; Rajanikant, G. K., Computational Identification of Novel Histone Deacetylase Inhibitors by Docking Based QSAR. *Comput. Biol. Med.* **2012**, *42* (6), 697-705. https://doi.org/10.1016/j.compbiomed.2012.04.001.

[23] Alzain, A. A.; Makki, A. A.; Ibraheem, W., Insights into the Inhibition of Mycolic Acid Synthesis by Cytosporone E Derivatives for Tuberculosis Treatment Via an In Silico Multi-Target Approach. *Chem. Africa* **2023**, *6* (4), 1811-1831. https://doi.org/10.1007/s42250-023-00605-7.

[24] Laoud, A.; Ferkous, F.; Maccari, L.; Maccari, G.; Saihi, Y.; Kraim, K., Identification of Novel Nt-MGAM Inhibitors for Potential Treatment of Type 2 Diabetes: Virtual Screening, Atom Based 3D-QSAR Model, Docking Analysis and ADME Study. *Comput. Biol. Chem.* **2018**, *72*, 122-135. https://doi.org/10.1016/j.compbiolchem.2017.12.003.

[25] El Mchichi, L.; Belhassan, A.; Aouidate, A.; Ghaleb, A.; Lakhlifi, T.; Bouachrine, M., QSAR Study of New Compounds Based on 1,2,4-Triazole as Potential Anticancer Agents. *Phys. Chem. Res.* **2020**, *8* (1), 125-

137. https://doi.org/10.22036/pcr.2019.204753.1685.

[26] Chaudhari, P.; Bari, S. In Silico Exploration of C-KIT Inhibitors by Pharmaco-Informatics Methodology: Pharmacophore Modeling, 3D QSAR, Docking Studies, and Virtual Screening. *Mol. Divers.* **2016**, *20* (1), 41-53. https://doi.org/10.1007/s11030-015-9635-x.

[27] Sharma, M. K.; Murumkar, P. R.; Kuang, G.; Tang, Y.; Yadav, M. R., Identifying the Structural Features and Diversifying the Chemical Domain of Peripherally Acting CB1 Receptor Antagonists Using Molecular Modeling Techniques. *RSC Adv.* **2016**, *6* (2), 1466-1483. https://doi.org/10.1039/C5RA20612J.

[28] Ouassaf, M.; Belaidi, S.; Khamouli, S.; Belaidi, H.; Chtita, S., Combined 3D-QSAR and Molecular Docking Analysis of Thienopyrimidine Derivatives as Staphylococcus Aureus Inhibitors. *Acta Chim. Slov.* **2021**, *68* (2), 289-303. https://doi.org/10.17344/acsi.2020.5985.

[29] Chiem, K.; Jani, S.; Fuentes, B.; Lin, D. L.; Rasche, M. E.; Tolmasky, M. E., Identification of an Inhibitor of the Aminoglycoside 6′-N-Acetyltransferase Type Ib [AAC(6′)-Ib] by Glide Molecular Docking. *Medchemcomm* **2016**, *7* (1), 184-189. https://doi.org/10.1039/C5MD00316D.

[30] Chahbaoui, N.; Khamouli, S.; Alaqarbeh, M.; Belaidi, S.; Sinha, L.; Chtita, S.; Bouachrine, M., Identification of Novel Curcumin Derivatives against Pancreatic Cancer: A Comprehensive Approach Integrating 3D-QSAR Pharmacophore Modeling, Virtual Screening, and Molecular Dynamics Simulations. *J. Biomol. Struct. Dyn.* **2023**, 1-19. https://doi.org/10.1080/07391102.2023.2266502.

[31] Ajay, D.; Sobhia, M. E., Simplified Receptor Based Pharmacophore Approach to Retrieve Potent PTP-LAR Inhibitors Using Apoenzyme. *Curr. Comput. Aided. Drug Des.* **2011**, *7* (3), 159-172. https://doi.org/10.2174/157340911796504288.

[32] Hu, Y.; Zhou, L.; Zhu, X.; Dai, D.; Bao, Y.; Qiu, Y., Pharmacophore Modeling, Multiple Docking, and Molecular Dynamics Studies on Wee1 Kinase Inhibitors. *J. Biomol. Struct. Dyn.* **2019**, *37* (10), 2703-2715. https://doi.org/10.1080/07391102.2018.1495576.

[33] Junaid, A.; Lim, F. P. L.; Tiekink, E. R. T.; Dolzhenko, A. V., Design, Synthesis, and Biological Evaluation of

New 6,N2-Diaryl-1,3,5-Triazine-2,4-Diamines as Anticancer Agents Selectively Targeting Triple Negative Breast Cancer Cells. *RSC Adv.* **2020**, *10* (43), 25517-25528. https://doi.org/10.1039/D0RA04970K.

[34] El Mchichi, L.; Tabti, K.; Kasmi, R.; El-Mernissi, R.; El Aissouq, A.; En-nahli, F.; Belhassan, A.; Lakhlifi, T.; Bouachrine, M., 3D-QSAR Study, Docking Molecular and Simulation Dynamic on Series of Benzimidazole Derivatives as Anti-Cancer Agents. *J. Indian Chem. Soc.* **2022**, *99* (9), 100582. https://doi.org/10.1016/j.jics.2022.100582.

[35] Ahmad, S.; Gupta, D.; Ahmed, T.; Islam, A., Designing of New Tetrahydro-β-Carboline-Based ABCG2 Inhibitors Using 3D-QSAR, Molecular Docking, and DFT Tools. *J. Biomol. Struct. Dyn.* **2023**, 1-12. https://doi.org/10.1080/07391102.2023.2176361.

[36] Lipinski, C. A., Rule of Five in 2015 and beyond: Target and Ligand Structural Limitations, Ligand Chemistry Structure and Drug Discovery Project Decisions. *Adv. Drug Deliv. Rev.* **2016**, *101*, 34-41. https://doi.org/10.1016/j.addr.2016.04.029.

[37] Gupta, S.; Bajaj, A. V., Extra Precision Glide Docking, Free Energy Calculation and Molecular Dynamics Studies of 1,2-Diarylethane Derivatives as Potent Urease Inhibitors. *J. Mol. Model.* **2018**, *24* (9), 261. https://doi.org/10.1007/s00894-018-3787-4.

[38] Mirzaei, S.; Ghodsi, R.; Hadizadeh, F.; Sahebkar, A., 3D-QSAR-Based Pharmacophore Modeling, Virtual Screening, and Molecular Docking Studies for Identification of Tubulin Inhibitors with Potential Anticancer Activity. *Biomed. Res. Int.* **2021**, *2021*, 6480804. https://doi.org/10.1155/2021/6480804.